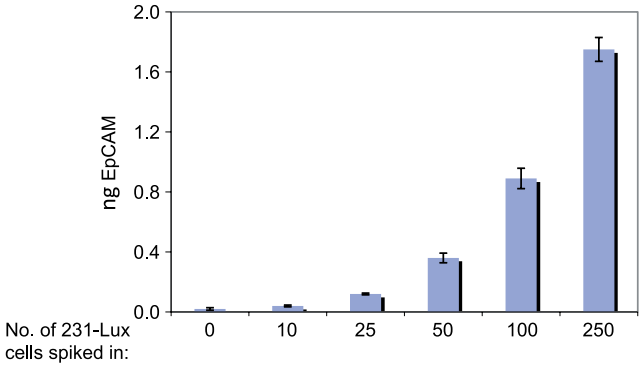


**Figure W1.** qPCR analysis of EpCAM levels in genomic DNA extracted from blood collected from naïve mice that was spiked with increasing numbers of human 231-Lux cells, as indicated. Bar graphs represent the averages ± SEM of replicates in a representative experiment.

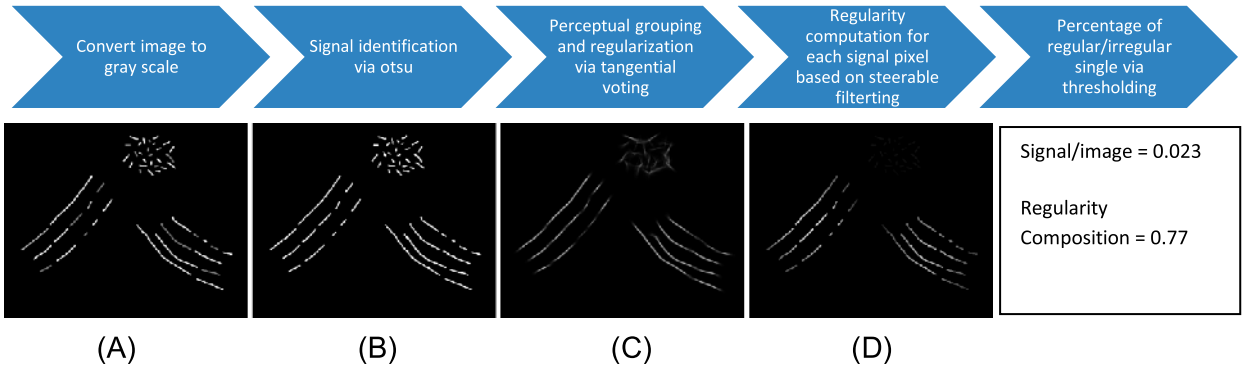


**Figure W2.** The workflow for quantification of regularity on a synthetic image: (A) the grayscale image converted from RGB space; (B) signal is thresholded and the percentage of collagen is computed per image; (C) perceptual gaps are filled through tangential voting; and (D) an index for each pixel that correlates with regularity in pattern formation is computed.

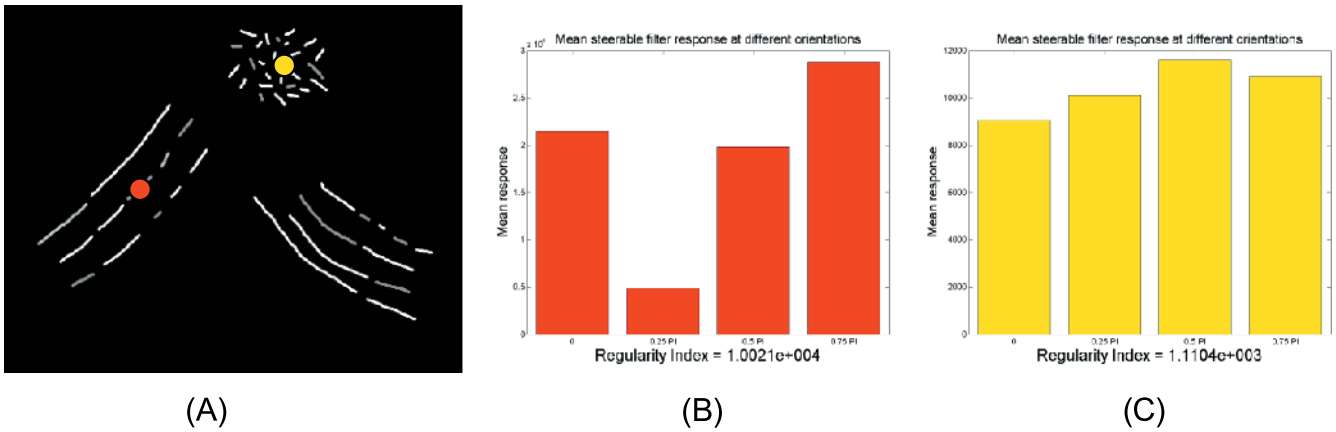


**Figure W3.** Construction of the regularity index on a synthetic image computed with four orientations of a steerable filter bank: (A) a synthetic image with regular and irregular fibers, where two points (red and yellow) are selected; (B) mean steerable filter responses at each of the four orientations for the red point; and (C) mean steerable filter responses for each of the four orientations for the yellow point. These examples show that a regular structure has much larger variance of steerable filter responses along different orientations than an irregular structure.

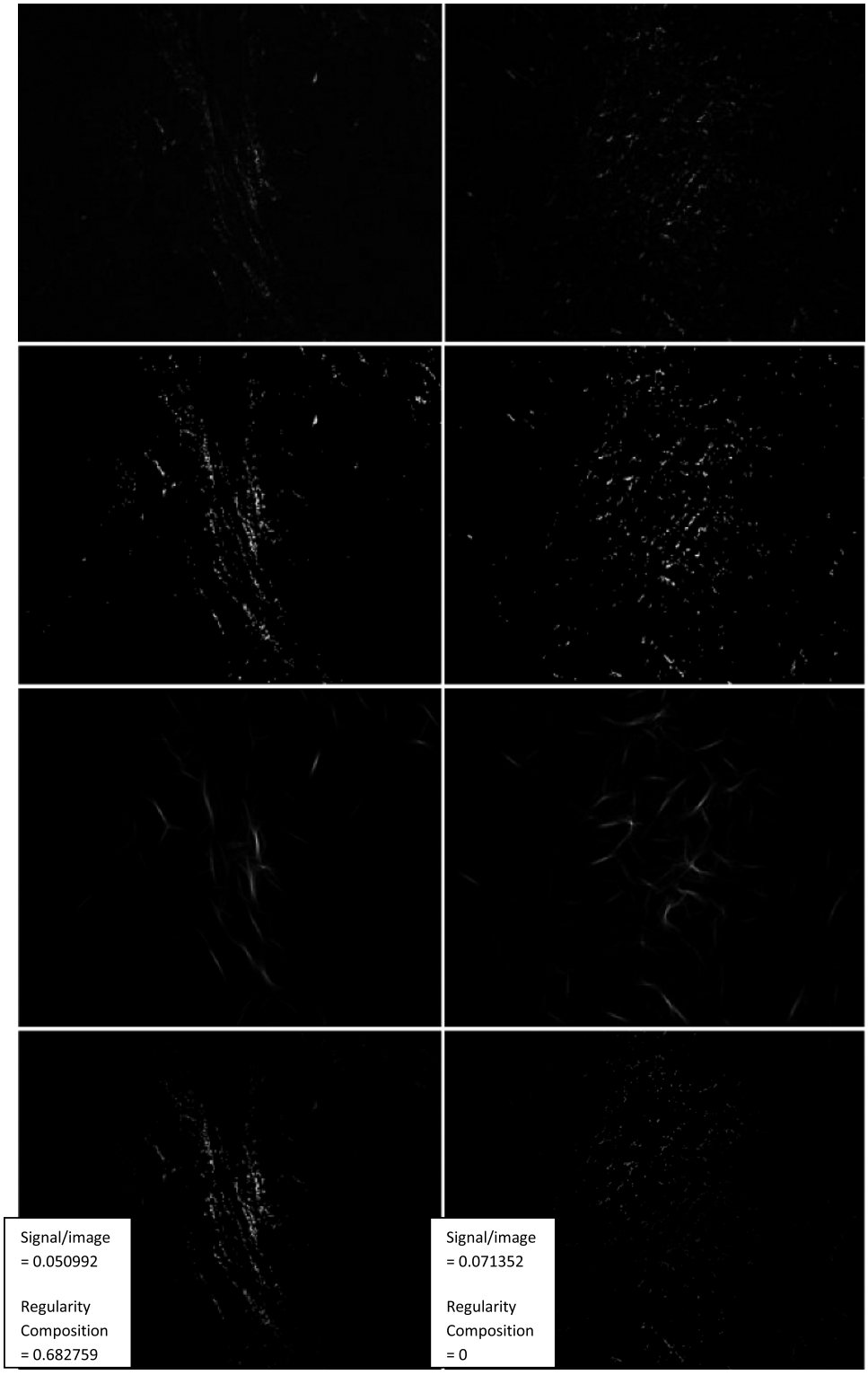


**Figure W4.** Examples of the quantification of the regularity composition index on a pair of real data. First row (top): The grayscale images converted from RGB space. Second row: Thresholded signal where the percentage of collagen is also computed. Third row: As a result of tangential voting, thresholded signal becomes more continuous and small gaps are filled. Fourth row: Computed regularity index for each pixel indicates that the image on the left has a higher regularity composition index.

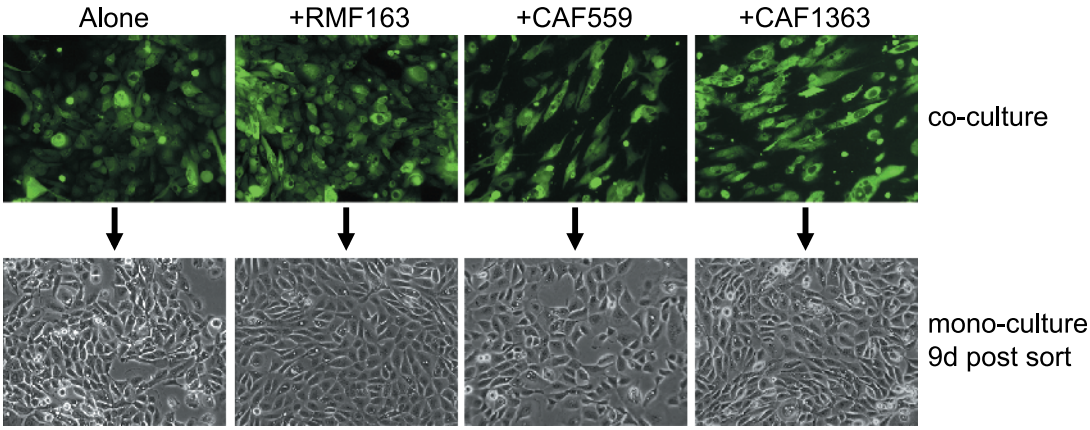


**Figure W5.** Representative 10× images of vHMEC-ras0.5 cells cultured alone or in combination with fibroblasts for 3 days (top row), and after they were isolated from the co-cultures and replated on their own in the absence of fibroblasts (bottom row) demonstrating that continued exposure to CAFs, or the ECM they deposit, is required for the maintenance of the aligned mesenchymal phenotype.

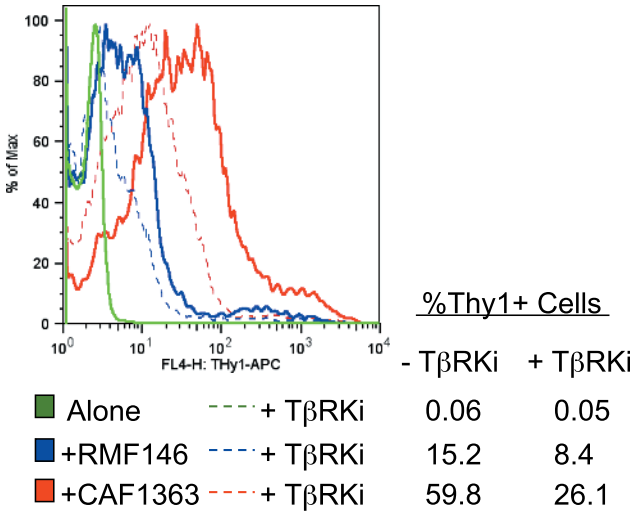


**Figure W6.** Flow cytometric analysis of Thy-1 expression in vHMEC-ras0.5 cells cultured either alone or with fibroblasts in the absence or presence of the TβRKi demonstrating that blockade of the CAF-induced mesenchymal phenotype is associated with a corresponding decrease in Thy-1 expression.

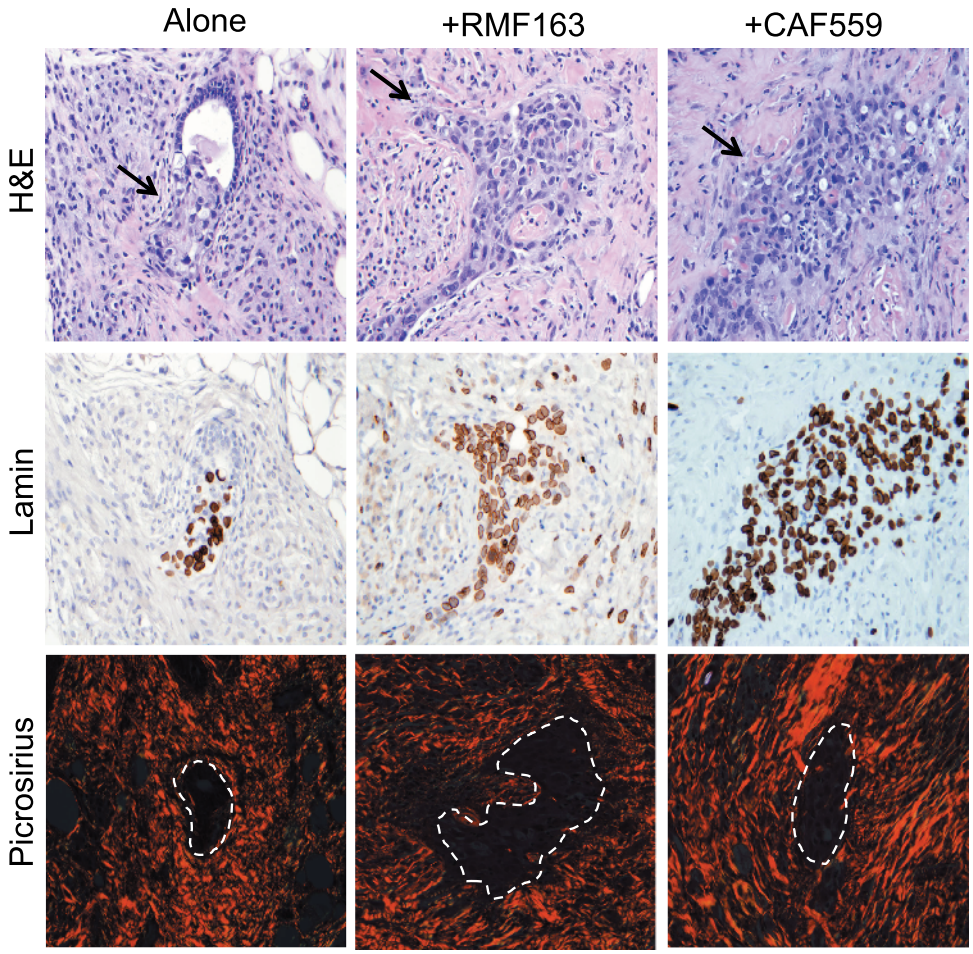


**Figure W7.** Higher magnification images of the H&E, lamin, and picrosirius stains shown in Figure 4.

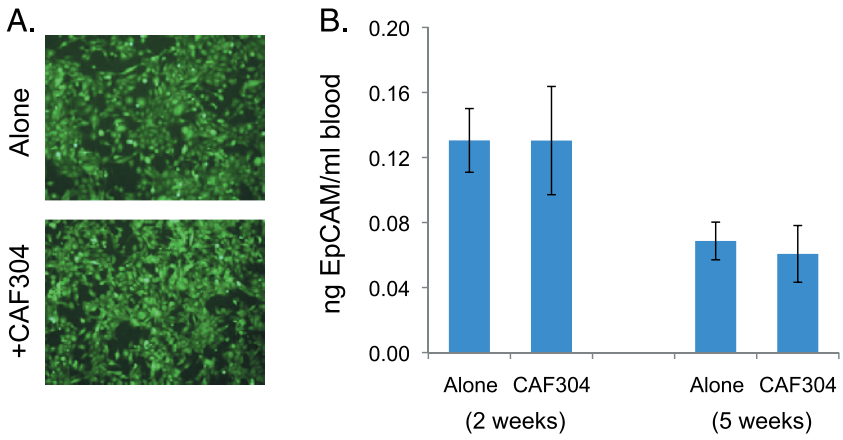


**Figure W8.** (A) Representative 10× images of vHMEC-ras0.5 cells cultured alone or with CAF304 for 3 days. (B) qPCR analysis of EpCAM levels in genomic DNA extracted from blood collected 2 and 5 weeks following orthotopic injection of $1 \times 10^6$ ras0.5-GFPLux cells alone ($n = 6$) or in combination with $3 \times 10^6$ CAF304 ($n = 6$). Blood was collected from three mice at each time point. Bar graphs represent the averages ± SEM of replicates in each experiment.

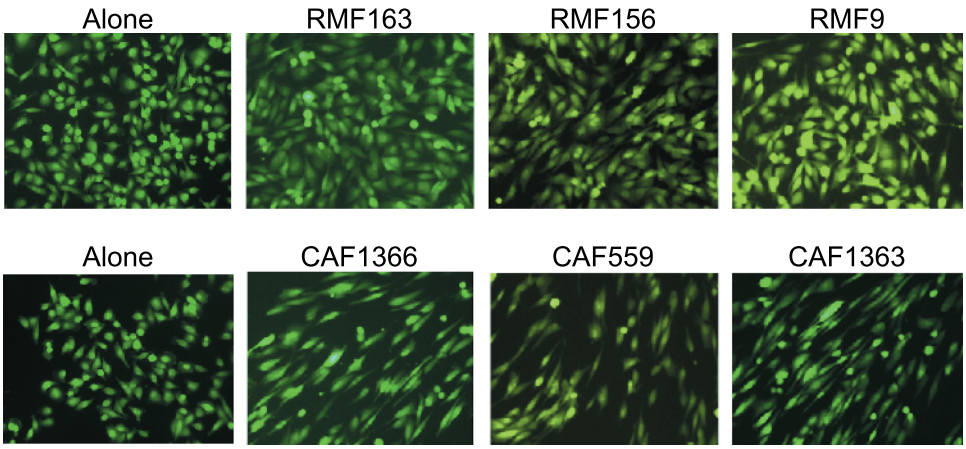


**Figure W9.** Representative 10× images of MDA-MB-231 cells co-cultured with RMFs or CAFs for 3 days.

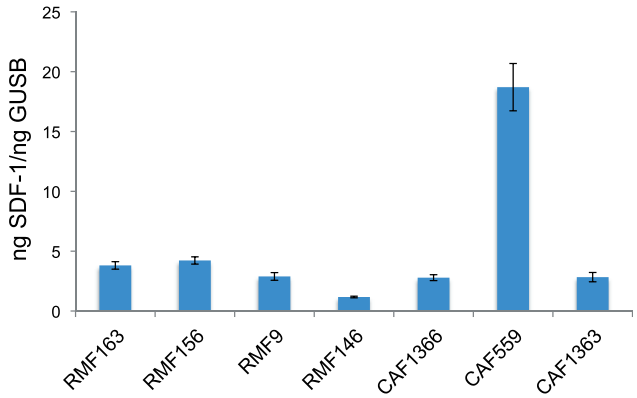


**Figure W10.** qPCR analysis of SDF-1 mRNA expression in RMFs and CAFs indicating that SDF-1 is only elevated in CAF559, which is the only CAF that stimulated primary tumor growth.

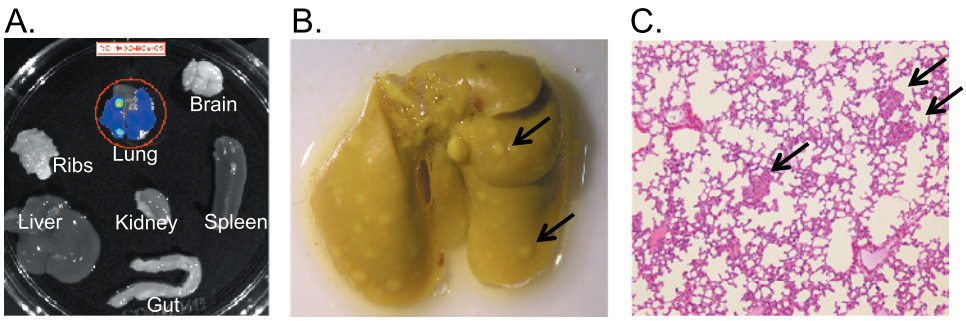


**Figure W11.** Representative images of (A) organs subjected to bioluminescence imaging *ex vivo* to quantify metastatic burden, (B) whole lung fixed in Bouin's for enumeration of surface metastases, and (C) H&E-stained lung section confirming the presence of pulmonary metastases. Arrows point to examples of metastatic nodules.